On the vertical structure of adiabatic wave forcing for the ocean circulation. Part I: Theory and practical implementation

Anne-Claire Bennis, Fabrice Ardhuin, Franck Dumas

On the vertical structure of adiabatic wave forcing for the ocean circulation
Part I: Theory and practical implementation

Anne-Claire Bennis[a], Fabrice Ardhuin[b], Franck Dumas[c]

[a] *UMR EPOC, Talance, France*
[b] *Laboratoire d'Océanographie Spatiale, Ifremer, 29200 Plouzané*
[c] *Laboratoire de Physique et Dynamique Sédimentaire, Ifremer, 29200 Plouzané*

Abstract

The conservation of momentum, when averaged over the phase of surface gravity waves can take two forms, whether or not the momentum variable contains the wave pseudo-momentum. Various published equations give different vertical profiles of the resulting wave-induced forces, even in adiabatic conditions. The differences for the total momentum equations are due to different approximations of the wave-induced vertical flux of momentum. These differences are made explicit for all wave-averaged equations, using a generic form of the conservation equations. The effects of these approximations is revealed here, for cases with exact numerical solutions, using a coupled wave-current three-dimensional model based on WAVEWATCH III (Tolman 1998, 2009) and MARS3D (Lazure and Dumas 2008). The necessary modifications of the MARS3D flow model are detailed, and may be applied to any other primitive equation model. In realistic conditions, all published models for the total momentum that are based on local wave quantities yield spurious velocities over a sloping bottom. Without any viscosity, these currents are independent of the slope. These spurious velocities are reduced but are still significant when a realistic vertical mixing is applied. It is concluded that models for the total momentum based on local wave quantities are likely to have large errors for cross-shore fluxes outside of the surf zone. Such errors are found using the equations from Mellor (2003) or Mellor (2008b). In the latter case, the depth-integrated equations also appear inconsistent. For all such models, the errors can be traced to inconsistent approximations of the vertical flux wave momentum. In contrast, the quasi-Eulerian mean momentum does not suffer from this inconsistency, and accurate numerical models

can be developed.

Keywords: wave-current coupling, radiation stresses, MARS3D, WAVEWATCH III

Three-dimensional oceanic flows can be strongly forced or modified by waves, in particular in the nearshore (e.g. Newberger and Allen, 2007a) and the coastal ocean (Lentz et al., 2008). Yet the numerical modelling of these complex flows is only slowly coming of age, with recent works using quasi-three dimensional (Haas et al., 2003) or fully three dimensional models (Uchiyama et al., 2009). Although models capable of resolving the wave motion are becoming feasible on small scales, as shown by Lubin et al. (2006), the demands of coastal zone management in terms of coverage and resolution are still barely met by depth-integrated models in which the wave motion is averaged over the phase of at least the short waves (e.g. Reniers et al., 2004). There has thus been a large effort to develop models of intermediate complexity, capable of resolving the vertical structure of the mean flow which may be needed to account for mixing and dispersion (Svendsen and Putrevu, 1994) while still keeping the hydrostatic approximation for the mean flow. Also, the wide community of users of numerical models for the ocean circulation such as POM and ROMS (Blumberg and Mellor, 1987; Shchepetkin and McWilliams, 2003) are calling for minor modifications to such tools to make them capable of representing the effects of waves.

A large body of often conflicting theoretical results have been published on the form of the wave-modified primitive equations that would be suitable for such models. We may cite, in chronological order, Dolata and Rosenthal (1984), Jenkins (1989), Weber and Melsom (1993), Rivero and Arcilla (1995), Péchon and Teisson (1994), Groeneweg and Klopman (1998), Mellor (2003), McWilliams et al. (2004), Xia et al. (2004), Newberger and Allen (2007b), Ardhuin et al. (2008b), Ardhuin et al. (2008a), Mellor (2008) ... Although each of these work is based on a particular set of hypotheses, for example some assume a horizontally uniform wave field, it is expected that all theories should agree on the most simple cases that they are supposed to cover. As we will show here, this is not the case.

Our purpose is not to blame this or that author for inconsistencies, limitations, or mistakes. The goal of the present paper is really to help people implement correctly the effect ot waves in a primitive equation model. We thus explain why some of the wave-averaged equations may appear different

but still represent correctly the same reality, and to give a general set of constraints that should be obeyed by wave-averaged equations so that each developer of a numerical model can make her or his own judgement of the published equations, sometimes even before implementing them.

Still, we will not escape our responsibility, and we shall point out specifically details or more important features that are not consistent in some of the most recent published results. We thus warn the many scientist that have chosen the equations by Mellor (2003, hereinafter M03) or Mellor (2008, hereinafter M08) that even the minor inconsistency in M03 or the larger one in M08 can produce strong artefacts. These artefacts are (re-)derived theoretically (see Ardhuin et al., 2008a, hereinafter AJB08, for a first discussion of M03), and illustrated using a coupled numerical model. Although these errors in the underlying theoretical model are likely to be dwarfed by parametrization errors in the case of strongly dissipative environments like the surf zone, they may still explain some of the differences found between various models (e.g. Haas and Warner, 2009).

We also take the present opportunity to present the approximated Generalized Lagrangian Mean equations ($glm2-z$) by Ardhuin et al. (2008b) (hereinafter ARB08) in a more readable form, giving details on how they were implemented in the MARS3D (Lazure and Dumas, 2008) flow model, used here. These steps have already been pioneered by McWilliams et al. (2004) and Uchiyama et al. (2009) with equations that are mathematically consistent with those in Ardhuin et al. (2008b). Yet, these more theoretical presentation are often obscured by their desire to be more general and more complete. We shall thus here present the equations and implementation in the most simple form, as a modification of the primitive equations, warning the reader when the simplification causes a loss of generality.

We focus here on non-dissipative conditions where exact solutions are most easily found, and we refer to Uchiyama et al. (2010) for further discussion of wave breaking, mixing and bottom friction parametrizations.

1. Theoretical analysis of wave-averaged equations

The various published theories can be categorized according to two criteria (Figure 1). The most simple is the depth integration: the equations are integrated or not. For the depth-integrated equations, with some approximations related to wave non-linearity, the problem is clear. The momentum balance can take two forms (Longuet-Higgins and Stewart, 1964; Garrett,

1976; Smith, 2006). One form is for the total momentum in the water column (M in Phillips' 1977 notation), and the other is for the momentum of the mean flow only (M^m in Phillips 1977). As shown by Smith (2006), the two forms are equivalent, and one only has to be careful that the two momentum variables do not represent the same physical quantity. In the case of M, it is the mass transport velocity, which naturally arises when working with fluxes of well-mixed solutes. For the special case of a mean current $\overline{u}$ that is uniform below the level of wave troughs, the other is approximately $M^m = \rho_w \overline{u} D$ where D is the mean water depth and ρ_w is a depth-averaged water density. We note that the wave momentum[1] is simply the difference $M^w = M - M^m$, and it is a horizontal vector. Hence, M^m may be more closely related to the mean current measurable by a fixed instrument. This interpretation, however, has to be considered with caution, since there may be different ways to extend the definition of $\overline{u}$ from the trough to the crest level, as needed when one wishes to model the surf zone.

These details are usually happily forgotten when considering depth-integrated equations, but they cannot be avoided when one wishes to discretize these two sets of equations, for the total momentum $\rho_w U$ or the mean flow momentum $\rho_w \widehat{u}$. Just like in the two dimensional (2D) case, Andrews and McIntyre (1978) have derived exact equations for U and $\widehat{u}$ that are equivalent. Unfortunately these exact equations are highly implicit and must be translated into usable form, as was done by Groeneweg and Klopman (1998) for the total momentum form or Ardhuin et al. (2008a) for the mean flow momentum form.

Thus, at the same order of approximation, we cannot have more than two sets of equations, one for U and the other for $\widehat{u}$ and both are equivalent. Any other equation must have some internal inconsistencies. We shall illustrate this statement for M03 and M08, because these are the most widely used equations, and we leave it to the reader to do the same for, for example, Xia et al. (2004) or any other proposed set of equation.

Any theory for wave-averaged equations goes through three steps. First, the control volume in which the momentum is averaged must be defined. For depth-integrated equations, this is simply the full water column. For

[1]The wave pseudo-momentum is defined as a quantity that only involves the zero-mean displacement of the water particles, and may differ from other definitions that could include the mean flow response, as explained by McIntyre (1981). For simplicity, we shall call 'momentum' the pseudo-momentum.

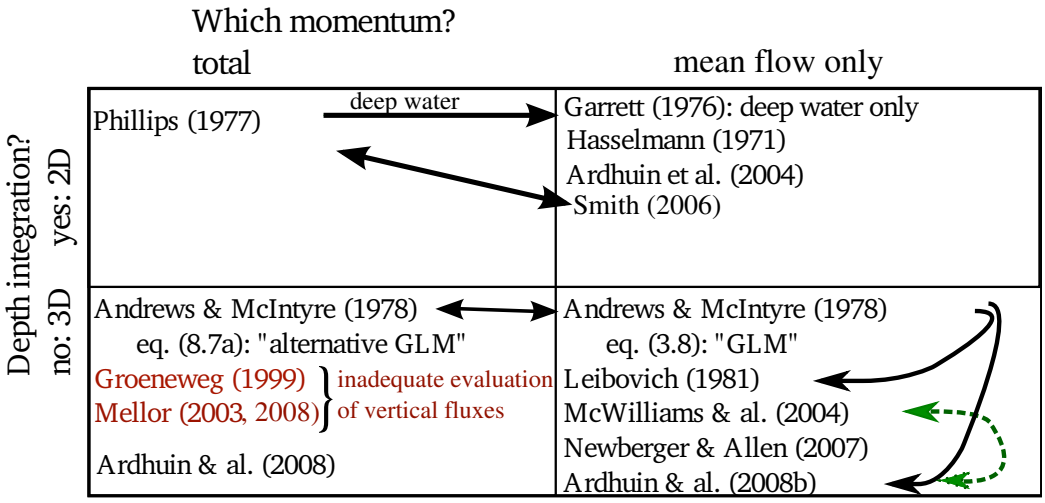

Figure 1: Relationships between wave-averaged theories according to their choice of momentum variable and depth integration. An arrow from a to b indicates a derivation link: b can be derived from a. In the case of McWilliams et al. (2004) and Ardhuin et al. (2008b), the second derivative in the vertical current profile is neglected in the second, while the first is only adiabatic. Names that appear in red correspond to theories that are not fully consistent with their originating hypotheses. In the case of 3D theories for the total momentum, the problem generally comes from the vertical flux of momentum and may only arise on a sloping bottom, not explicitly considered by Groeneweg (1999).

three-dimensional equations, there is a vertical discretization. The control volume may be moving, following all or part of the wave motion (Figure 2). The mean position $\mathbf{x} = (x, y, z)$ of the volume, is associated with the actual position

$$\mathbf{x} + \xi(x, y, z, t) = (x + \xi_1(x, y, z, t), y + \xi_2(x, y, z, t), z + \xi_3(x, y, z, t)) \,. \quad (1)$$

The boundaries of the volume at time t_0 are the surfaces $x = x_0 + \Delta + \xi_1(x_0 + \Delta, y, z, t_0)$, $y = y_0 + \Delta + \xi_2(x, y_0 + \Delta, z, t_0)$, and $z = z_0 + \Delta + \xi_3(x, y, z_0 + \Delta, t_0)$, with $\Delta = \Delta_z/2$ for the top, and $\Delta = -\Delta_z/2$ for the bottom surfaces, with similar definitions for the sides.

For the Eulerian average, the volume does not move, and $\xi = (\xi_1, \xi_2, \xi_3) = 0$. For the average defined by Mellor (2003), the horizontal displacements are zero, $\xi_1 = 0$ and $\xi_2 = 0$, and ξ_3 follows the wave motion.

Second, the momentum balance of the volume is the result of the body forces and the momentum fluxes through the boundary. These fluxes involves

an advective part (ρu^2 for the horizontal advection of horizontal momentum and ρuw for the vertical advection) and a stress part that is the product of the stress tensor with the unit vector normal to the boundary. Neglecting shear stresses for simplicity leaves only the pressure p for the stress. For $\xi \neq 0$, the control volumes have tilted facets, with a flux of horizontal momentum through the sloping bottom and top. The corresponding flux of the x-component of the momentum is $p\partial\xi_3/\partial x$. Fluxes due to sloping iso-coordinates are often forgotten (e.g. Xia et al. 2004, Mellor 2008b[2]) or poorly approximated (e.g. Mellor 2003).

Last, the averaged equations can be transformed to another coordinate system, such as terrain-following coordinates. Averaging can cause an implicit distortion of the coordinates, for example the mean flow may appear divergent although the original flow is not. This effect may be easily corrected (see e.g. Ardhuin et al., 2008b, for the transformation of approximated Generalized Lagrangian Mean equations to Cartesian and terrain-following coordinates).

Because of the large difference in density between air and water, the use of a standard Eulerian average, used by Rivero and Arcilla (1995) or Newberger and Allen (2007b) is problematic in the region between crests and trough where both air and water are to be found. A strict Eulerian average produces a continuously varying density ρ from about 1.29 kg.m^{-3} to 1026 kg.m^{-3}, which is not compatible with the usual primitive equation models. Mathematical extension of the velocity field across the interface have been used by McWilliams et al. (2004), but it provides quantities that are difficult to interpret physically since they do not a priori correspond to a known averaging operator. Yet, Ardhuin et al. (2008b) showed that the resulting velocity actually corresponds to the quasi-Eulerian velocity $(\widehat{u}, \widehat{v}, \widehat{w})$ first introduced by Jenkins (1989): this is the mean Lagrangian velocity (U, V, W) minus the wave-induced drift (U_s, V_s, W_s),

$$(\widehat{u}, \widehat{v}, \widehat{w}) = (U, V, W) - (U_s, V_s, W_s). \tag{2}$$

This definition requires a wave-following coordinate system. The averaging is also connected to the choice of the momentum variable, which varies between different theories, as summarized in Figure 1.

[2]In that work, the control volume is identical to the one in M03, but an Eulerian average of the pressure is taken, making the averaged equations inconsistent.

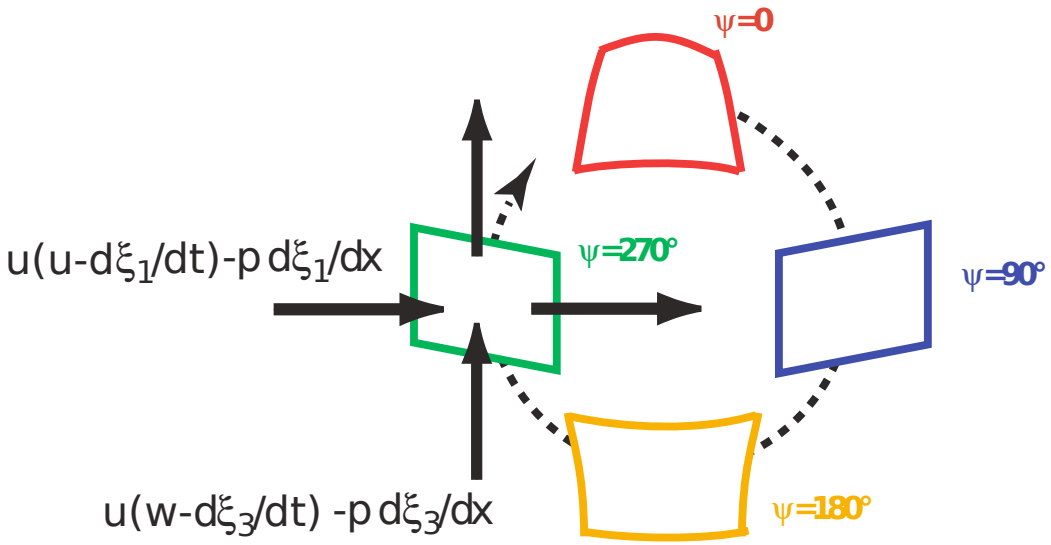

Figure 2: Illustration of the momentum fluxes into a moving control volume defined by the (possibly moving) position vector of the control volume, $\Xi(x, y, z, t) = \mathbf{x} + \xi$. Here the control volume moves in a circle and is shown for 4 wave phase, $\psi = 0°$, $\psi = 90°$, $\psi = 180°$ and $\psi = 270°$. The fluxes are the sum of advective fluxes through the facets and the pressure acting on the possibly sloping facets. For the advective part the velocity is relative to the moving facet, which leads to terms like $-u\partial\xi_3/\partial t$.

Neglecting buoyancy, Earth rotation, mixing and viscous effect, the generic conservation equation for the mean momentum $\overline{\rho u}$, with motion restricted to a vertical plane is

$$\frac{\partial(\overline{\rho u})}{\partial t} + \frac{\partial(\overline{\rho u}\ \overline{u})}{\partial x} + \frac{\partial(\overline{\rho u}\ \overline{w})}{\partial z} = F, \tag{3}$$

with F a forcing term due to waves and water levels.

The rate of change of the momentum (the first term on the left hand side of eq. 3) equals body forces (such as gravity, absent for the horizontal momentum ρu), plus the divergence of fluxes of momentum. The mean flow advective fluxes appear in the left hand side of (3), the other fluxes constitute the forcing term F. For a generic control volume, F is

$$F = F_{uu} + F_{uw} + F_{px} + F_{p3}, \tag{4}$$

with the horizontal advection

$$F_{uu} = \frac{\partial(\overline{\rho\widetilde{u}^2})}{\partial x}. \tag{5}$$

$\widetilde{u}$ is the horizontal velocity associated to the wave propagation such as

$$\widetilde{u} = kac\left[exp(kz)cos(kx - \sigma t)\right]. \tag{6}$$

where k is the wavenumber, a is the wave amplitude, c is the phase speed, σ is the frequency (More in Mellor (2003)).

The vertical advection (where $\widetilde{w}$ is the vertical velocity associated to the wave propagation such as $\widetilde{w} = kac\left[exp(kz)sin(kx - \sigma t)\right]$)

$$F_{uw} = \frac{\partial\left[\left(\widetilde{w} - \partial\widetilde{\xi}_3/\partial t\right)\rho\widetilde{u}\right]}{\partial(z + \xi_3)}, \tag{7}$$

is important for fixed (Eulerian) control volumes (e.g. Rivero and Arcilla, 1995) but is negligible for the M03-AJB08 volume, designed to make $\widetilde{w} - \partial\widetilde{\xi}_3/\partial t$ as small as possible.

The last two terms are the pressure gradient across the sides of the volume, here assumed vertical[3],

$$F_{px} = \overline{\frac{\partial p}{\partial x}}, \tag{8}$$

and the vertical divergence of the pressure-induced flux through the sloping iso-surfaces of the vertical coordinate,

$$F_{p3} = \frac{\partial S_{p3}}{\partial z} = \frac{\partial}{\partial z}\overline{\left[\widetilde{p}(\partial\widetilde{\xi}_3/\partial x)\right]}, \tag{9}$$

which is zero in Eulerian averages, for which $\widetilde{s} = 0$. We recall that $\overline{p}$ can be different for different control volumes, i.e. in the case of M03-AJB08 the pressure is nearly hydrostatic, which is not the case of a fixed control volume for which a $-\overline{\rho\widetilde{w}^2}$ correction occurs. So far the M03 theory is correct. Using the notations of that paper, $\widetilde{s} = \xi_3 = \widetilde{\xi}_3$, $\xi_1 = 0$, $\xi_2 = 0$.

1.1. Inconsistencies in M03

The equation of motion, where we have neglected the Coriolis force, density stratification, and mixing, are given by Mellor (2003) and correspond to

[3]These sides actually have an angle in the case of the Generalized Lagrangian Mean (GLM), giving more complex equations.

equation (3) that is similar to the following equation. Rewritten in a terrain following vertical coordinate, ς, it is

$$\frac{\partial U}{\partial t} + U\frac{\partial U}{\partial x} + \frac{W}{D}\frac{\partial U}{\partial \varsigma} = \frac{F}{D}. \tag{10}$$

The force on the right hand side is the sum

$$F = F_{uu} + F_{px} + F_{p3} \tag{11}$$

of the hydrostatic pressure gradient, $F_{px} = -gD\dfrac{\partial \widehat{\eta}}{\partial x}$, with $\widehat{\eta}$ the mean surface elevation, and the divergences of the horizontal and vertical fluxes of momentum, F_{uu} and F_{p3}, given in Appendix D. Because Mellor (2003) used only Airy theory over a flat bottom to solve for the wave motion, he obtained an erroneous estimation of F_{p3} (see Appendix D). Over a sloping bottom in finite water depth, F_{uu} is of the order of the bottom slope ε_2, and a consistent solution of eq. (3) requires an approximate of F_{p3} to the same order. This requires $O(\varepsilon_2)$ estimates of both $\widetilde{p}$ and $\widetilde{s}$, for which Airy theory, used by M03, is not sufficient. As a result the total force F according to Mellor (2003) integrates to zero over the vertical, but it has a vertical profile that can exceeds 150% of the pressure gradient F_{px}, instead of the correct value of zero. A correct but prohibitively expensive numerical method for the estimation of F_{p3} was given by AJB08. AJB08 showed that this problem with F_{p3} arises from the wave momentum flux. This difficulty is thus absent from equations for the quasi-Eulerian momentum $\widehat{u}$, which does not contain the wave momentum.

1.2. Inconsistencies in M08

The equations of motion for the M08 model are similar to (10) based on the same vertical coordinate ς but with a different forcing F at the lowest order. Thus one of the two equations is incorrect. Since (10) was verified by Ardhuin et al. (2008b) with a proper approximation of the different terms, it follows that M08 must be incorrect. Let us see why. The forcing term for a generic control volume is given by equation (4). In comparison with the M03 model, F_{p3} is absent and F_{px} includes an additional Eulerian-like pressure correction ($F_{px}^{M08,\,\mathrm{add}}$) defined by

$$F_{px}^{M08,\mathrm{add}} = \varsigma\frac{\partial D}{\partial x}\frac{\partial S_{xx}^{M08,\,\mathrm{add}}}{\partial \varsigma}, \tag{12}$$

with the additional radiation stress term in x-direction ($S_{xx}^{M08,\,\mathrm{add}}$)

$$S_{xx}^{M08,\,\mathrm{add}} = -kEF_{SC}F_{SS} + E_D, \tag{13}$$

where E is the wave energy, F_{SS} and F_{SC} are non-dimensional functions of kz and kD (see M03). E_D is defined by

$$E_D = 0 \text{ if } z \neq \widehat{\eta} \text{ and } \int_{-h}^{\widehat{\eta}^+} E_D dz = \frac{E}{2}, \tag{14}$$

where h is the depth at the bottom and $\widehat{\eta}$ is the mean surface elevation.

The M08 radiation tensor term in x-direction (S_{xx}^{M08})contains the usual term from the velocity squared, but now also the $S_{xx}^{M08,\,\mathrm{add}}$ term,

$$S_{xx}^{M08} = \underbrace{kE\left[\frac{k_x^2}{k^2}F_{CS}F_{CC}\right]}_{\text{as in M03}} \underbrace{-kEF_{SC}F_{SS} + E_D}_{S_{xx}^{M08,\,\mathrm{add}}\text{ term}}. \tag{15}$$

Mellor (2008) mentions that the vertical integral $\int_{-h}^{\widehat{\eta}} S_{xx}^{M08} dz$ is equal to the S_{xx}^{P77} term given by Phillips (1977),

$$\int_{-h}^{\widehat{\eta}} S_{xx}^{M08} dz = S_{xx}^{P77} = E\left[\left(\frac{k_x^2}{k^2}\right)\cdot\left(\frac{c_g}{c}\right) + \left(\frac{c_g}{c} - \frac{1}{2}\right)\right], \tag{16}$$

where c_g is the group velocity and c is the phase velocity.

This is very well, but the depth-integration of the M08 model does not correspond to Phillips (1977) because the forcing is not S_{xx}^{P77} but $\partial S_{xx}^{P77}/\partial x$. Namely,

$$\begin{aligned}\int_{-h}^{\widehat{\eta}} \frac{\partial S_{xx}^{M08}}{\partial x} dz &= \frac{\partial S_{xx}^{P77}}{\partial x} - S_{xx}^{M08}(z=-h)\frac{\partial h}{\partial x} \\ &\quad - S_{xx}^{M08}(z=\widehat{\eta})\frac{\partial \widehat{\eta}}{\partial x}.\end{aligned} \tag{17}$$

Thus the depth integration of the M08 equation give a spurious acceleration $S_{xx}^{M08}(z=-h)\partial h/\partial x$ that can be very large.

2. Equations for the quasi-Eulerian momentum

In order to facilitate the implementation of quasi-Eulerian equations, we give here a short and simplified account of Ardhuin et al. (2008b). Starting from the general equations of Andrews and McIntyre (1978), Ardhuin et al. (2008b) have given an approximation to second order in the wave non-linearity and transformed the equations with a change of the vertical coordinate, so that the Jacobian associated with the averaging procedure is equal to identity, and both the resulting quasi-Eulerian flow field $(\widehat{u}, \widehat{v}, \widehat{w})$ and Lagrangian-mean flow field (U, V, W) are non-divergent.

The quasi-Eulerian flow field does not contain wave momentum, and this is the main difference with the M03 and M08 models that apply to the Lagrangian flow field which does contain the wave momentum. Solving $(\widehat{u}, \widehat{v}, \widehat{w})$ removes the problem of the approximation of the vertical fluxes of wave momentum that occur when wave propagation over varying currents and water depths. The influence of waves on the mean quasi-Eulerian current appear as forcing terms (A1, A2, B1, B2, C1, C2, C3 in the equations (18),(19),(21)).

We shall here consider the case in which the wave bottom boundary layer is not resolved. For a discussion of this, see Ardhuin et al. (2008a). To simplify the equations we generally give the wave forcing expressions for monochromatic waves as a function of the surface elevation variance E. In the case of quasi-linear random waves the corresponding forcing is simply the sum of the monochromatic wave forcing with E replaced by the spectral density $E(f, \theta)$, as detailed in Appendix C. The following GLM equations use the Cartesian z coordinate. However, the most of coastal hydrodynamical models use equations in terrain-following coordinates, then we detailed these equations for MARS3D in Appendix A. We notice that the classical formulation of the advection terms in momentum equations allow for straightforward numerical implementation of the vortex terms. On the other hand, the coastal hydrodynamical models make frequent use of flux-divergence formulation of the advection terms in momentum equations (Marsaleix et al. (2008), Blumberg and Mellor (1987), Shchepetkin and McWilliams (2004)). Even though the momentum equations for the both formulations of advection terms are equivalent, the expressions of (U_s, V_s, W_s) depending forces has been modified (see Appendix B).

2.1. Momentum, mass, and tracer conservation

For simplicity we neglect the effect of the vertical current shear and partial standing waves in the wave forcing term, so that eq. (42) in Ardhuin et al. (2008b) becomes

$$\begin{aligned}\frac{\partial \widehat{u}}{\partial t} &+ \widehat{u}\frac{\partial \widehat{u}}{\partial x} + \widehat{v}\frac{\partial \widehat{u}}{\partial y} + \widehat{w}\frac{\partial \widehat{u}}{\partial z} - f\widehat{v} + \frac{1}{\rho}\frac{\partial p^H}{\partial x} \\ &= \underbrace{\widehat{F}_{m,x} + \left[f + \left(\frac{\partial \widehat{v}}{\partial x} - \frac{\partial \widehat{u}}{\partial y}\right)\right] V_s - W_s \frac{\partial \widehat{u}}{\partial z}}_{A1} \underbrace{- \frac{\partial J}{\partial x} + \widehat{F}_{d,x} + \widehat{F}_{b,x}}_{A2}, \quad (18)\end{aligned}$$

and

$$\begin{aligned}\frac{\partial \widehat{v}}{\partial t} &+ \widehat{u}\frac{\partial \widehat{v}}{\partial x} + \widehat{v}\frac{\partial \widehat{v}}{\partial y} + \widehat{w}\frac{\partial \widehat{v}}{\partial z} + f\widehat{u} + \frac{1}{\rho}\frac{\partial p^H}{\partial y} \\ &= \underbrace{\widehat{F}_{m,y} - \left[f + \left(\frac{\partial \widehat{v}}{\partial x} - \frac{\partial \widehat{u}}{\partial y}\right)\right] U_s - W_s \frac{\partial \widehat{v}}{\partial z}}_{B1} \underbrace{- \frac{\partial J}{\partial y} + \widehat{F}_{d,y} + \widehat{F}_{b,y}}_{B2}, \quad (19)\end{aligned}$$

where the left hand side is the classical primitive equation model for the quasi-eulerian velocity $(\widehat{u}, \widehat{v}, \widehat{w})$ with p^H the hydrostatic pressure, $(\widehat{F}_{m,x}, \widehat{F}_{m,y})$ the mixing effects (that redistribute momentum), $(\widehat{F}_{d,x}, \widehat{F}_{d,y})$ the source of quasi-Eulerian momentum that is equal to the sink of wave momentum due to breaking and wave-turbulence interaction, $(\widehat{F}_{b,x}, \widehat{F}_{b,y})$ the source of quasi-Eulerian momentum that is equal to the sink of wave momentum due to bottom friction, which should only be included when the wave bottom boundary layer is resolved, J the wave-induced mean pressure (eq. (26)), and (U_s, V_s, W_s) the three-dimensional Stokes drift[4]. Mixing is also influenced by waves, but this aspect will not be discussed here (see Craig and Banner, 1994; Groeneweg and Klopman, 1998; Rascle and Ardhuin, 2009; Uchiyama et al., 2010). The second lines in eq. (18)–(19) contain the vortex force introduced

[4]Although the vertical component of the Stokes drift may not be familiar to the reader, it appears, just like the horizontal components, in the general definition of the wave pseudo-momentum (Andrews and McIntyre, 1978; Ardhuin et al., 2008b). In particular for inviscid conditions over a sloping bottom it is physically obvious that the drift of water particles must follow the bottom and thus must have a vertical component. In practice W_s can be computed from (U_s, V_s) as the full Stokes drift flow is non-divergent (Ardhuin et al., 2008b)

by Garrett (1976) in this context, and further discussed by Lane et al. (2007) and Smith (2006).

The mass conservation is

$$\frac{\partial \widehat{u}}{\partial x} + \frac{\partial \widehat{v}}{\partial y} + \frac{\partial \widehat{w}}{\partial z} = 0, \tag{20}$$

and the evolution of a conservative passive tracer concentration $\mathcal{C}$ is,

$$\frac{\partial \mathcal{C}}{\partial t} + \frac{\partial}{\partial x}\left[(\widehat{u} + \underbrace{U_s}_{C1})\mathcal{C}\right] + \frac{\partial}{\partial y}\left[(\widehat{v} + \underbrace{V_s}_{C2})\mathcal{C}\right] + \frac{\partial}{\partial z}\left[(\widehat{w} + \underbrace{W_s}_{C3})\mathcal{C}\right] = 0. \tag{21}$$

All four conservation equations are valid from the bottom $z = -h$ to the local phase-averaged free surface $\widehat{\eta}$.

However, with the mode splitting, there is another important modification that is made through the barotropic mode. The surface kinematic boundary condition is given by

$$\frac{\partial \widehat{\eta}}{\partial t} + (\widehat{u} + U_s)\frac{\partial \widehat{\eta}}{\partial x} + (\widehat{v} + V_s)\frac{\partial \widehat{\eta}}{\partial y} = \widehat{w} + W_s. \tag{22}$$

It thus appears that, as in McWilliams et al. (2004) or Newberger and Allen (2007b) there is a source of mass at the surface that compensates the convergence of the Stokes drift. In surface-following coordinates there is no velocity through the surface and $\widehat{w} + W_s$ vanish, leaving only the convergence of the Stokes drift to force the usual mass conservation equation (see Appendix A: eq. (A.3)).

For tracers, because the equations are unchanged (only for the explicit appearance of the Lagrangian mean velocity), the boundary conditions are unchanged from classical primitive equation models.

2.2. Wave-induced forcing terms

The three-component Stokes drift (U_s, V_s, W_s), wave-induced pressure term J, and momentum source due to wave dissipation $(\widehat{F}_{d,x}, \widehat{F}_{d,y})$, can all be computed from only a few local parameters. These include the wave-induced surface elevation variance E, the phase-averaged water depth $D = h + \widehat{\eta}$, the wavenumber vector $\mathbf{k} = k(\cos\theta, \sin\theta)$, the intrinsic radian frequency $\sigma = \sqrt{gk\tanh(kD)}$, the water depth D. For random waves, these expression

are easily extended by summing over the spectrum and replacing E by the spectral density $E(f,\theta)$ (see Appendix C).

The horizontal Stokes drift vector (U_s, V_s) is given by,

$$(U_s, V_s) = \sigma k(\cos\theta, \sin\theta) E \frac{\cosh(2kz+2kh)}{\sinh^2(kD)}. \tag{23}$$

At the lowest order, the full Stokes drift flow is non-divergent and verify,

$$\frac{\partial U_s}{\partial x} + \frac{\partial V_s}{\partial y} + \frac{\partial W_s}{\partial z} = 0. \tag{24}$$

As a result, the less well-known vertical Stokes drift component is given, at lowest order (e.g. Ardhuin et al., 2008a), by the horizontal divergence of (U_s, V_s),

$$W_s(z) = -\left.U_s\right|_{z=-h} \frac{\partial h}{\partial x} - \left.V_s\right|_{z=-h} \frac{\partial h}{\partial y} - \int_{-h}^{z} \frac{\partial U_s}{\partial x} + \frac{\partial V_s}{\partial y} \mathrm{d}z. \tag{25}$$

In adiabatic conditions, the only other term is the wave-induced mean pressure J,

$$J = g\frac{kE}{\sinh 2kD}. \tag{26}$$

In the coupled system, the horizontal Stokes velocity is computed in the coupler from the frequency spectrum of the surface Stokes drift, which is provided by WWATCH, so that the wave model does not need to know the depths of the flow model levels. This also allows to force the flow model with a stored wave output that is independent of the flow model vertical resolution (see http://tinyurl.com/2wr6hoa for details). The vertical component W_s is obtained by solving equation (25).

No definite theory exists for the force induced by wave dissipation $(\widehat{F}_{d,x}, \widehat{F}_{d,y})$, as only the depth-integrated force is known (e.g. Smith, 2006). An empirical parametrization for the vertical profile must be used. We may clearly distinguish between the force due to wave breaking and that due to bottom dissipation (Walstra et al., 2000). We know S_{oc} the amount of energy given up by waves as they break, either in finite depth or deep water (e.g. Thornton and Guza, 1983; Ardhuin et al., 2009b), and S_{bf} the loss of energy due to bottom friction (Ardhuin et al., 2003b, e.g.). With a strong vertical mixing due to breaking waves the vertical distribution of the momentum source is not very important (Rascle et al., 2006). One may parametrize the effect of

wave dissipation as a surface stress, with a vertical profile given by the delta function $\delta_{z,\widehat{\eta}}$,

$$\begin{aligned}(\widehat{F}_{d,x},\widehat{F}_{d,y})(z) &= (\tau_{oc,x},\tau_{oc,x})\delta_{z,\widehat{\eta}} \\ &= \int \frac{k}{\sigma}(\cos\theta,\sin\theta)S_{oc}(f,\theta)\delta_{z,\widehat{\eta}}\mathrm{d}f\mathrm{d}\theta,\end{aligned} \tag{27}$$

where $S_{oc}(f,\theta)$ is the spectral density of the waves-to-ocean energy flux (e.g. Ardhuin et al., 2009b), approximately equal to the dissipation source function in the spectral wave energy balance. We have rather used a linear profile for $(\widehat{F}_{d,x},\widehat{F}_{d,y})$, spread over a vertical distance of $\dfrac{H_{rms}}{2}$ (Walstra et al., 2000).

2.3. Boundary conditions at the bottom

The bottom friction is absent in the test cases presented here. However, for case with bottom friction, the following equations can be used.

Starting from the bottom, at $z=-h$, **for a non-resolved wave bottom boundary layer**, the momentum lost by waves due to bottom friction is lost in the bottom (Longuet-Higgins, 2005) and should not be added in the water column, and the horizontal velocity should be prescribed as velocity at the bottom given by the streaming solution of (Longuet-Higgins, 1953), still approximately valid for turbulent bottom boundary layers (e.g. Marin, 2004),

$$(\widehat{u},\widehat{v})|_{z=-h} = 1.5\ (U_s,V_s)|_{z=-h} \tag{28}$$

and the vertical velocity is naturally

$$\widehat{w} = -\widehat{u}\frac{\partial h}{\partial x} - \widehat{v}\frac{\partial h}{\partial y}. \tag{29}$$

If the **wave bottom boundary layer were resolved** then the bottom stress can be parametrized as

$$K_z\frac{\partial\widehat{u}}{\partial z} = \frac{\kappa^2}{\ln\left[(z+h)/z_0\right]}\Delta_u\sqrt{\Delta_u^2+\Delta_v^2} \tag{30}$$

where $\Delta_u=\widehat{u}(z)$ and $\Delta_v=\widehat{v}(z)$, and K_z is the (varying) eddy viscosity. The vertical velocity is given by equation (29).

In this case, one should introduce the source of momentum

$$(\widehat{F}_{b,x}, \widehat{F}_{b,y})(z) = \int \frac{k}{\sigma}(\cos\theta, \sin\theta) S_{bf}(f,\theta) G(z) \mathrm{d}f \mathrm{d}\theta, \tag{31}$$

near the bottom, where $G(z)$ is a function that integrates to 1 across the wave bottom boundary layer. This may be re-written

$$(\widehat{F}_{b,x}, \widehat{F}_{b,y})(z) = (\tau_{wb,x}, \tau_{wb,x}) G(z). \tag{32}$$

The wave bottom stress vector $(\tau_{wb,x}, \tau_{wb,x})$ corresponds to the momentum lost by the wave field via bottom friction and can be computed by the wave model. The vertical distribution function $G(z)$ can be parameterized from the bottom displacement a_{orb}, the bottom roughness z_0 and a friction factor f_w which can also be computed by the wave model (e.g. Ardhuin et al., 2003a; Walstra et al., 2000). Another important condition is the energy lost by waves due to bottom friction which is a source of turbulent kinetic energy in the bottom boundary layer. The total energy is the same integral as eq. (31), without the $\dfrac{k}{\sigma}$ factor and a profile that can be parametrized following Mellor (2002).

2.4. Boundary conditions at the surface

At the surface, the stresses are imposed, giving the upper boundary condition for the turbulent momentum flux,

$$K_z \frac{\partial \widehat{u}}{\partial z} = \tau_{a,x} - \tau_{aw,x} \tag{33}$$

where $\tau_{a,x}$ and $\tau_{aw,x}$ are, respectively, the x-component of the wind stress and of the wave-supported stress

$$(\tau_{aw,x}, \tau_{aw,y}) = \int \frac{k}{\sigma}(\cos\theta, \sin\theta) S_{atm}(f,\theta) \mathrm{d}f \mathrm{d}\theta, \tag{34}$$

where $S_{atm}(f,\theta)$ is the spectral density of the wind to wave energy flux (e.g. Ardhuin et al., 2009a), approximately equal to the input source function in the spectral wave energy balance. Here again the other boundary condition for the flux of turbulent kinetic energy is given by loss of wave energy due to breaking and wave-turbulence interaction the same integral as (27) without the $\dfrac{k}{\sigma}$ factor, and it may also be distributed as a near-surface source.

2.5. Lateral boundary conditions

When open boundary conditions are used, one may impose a zero mass flux to facilitate the numerical convergence (Rascle, 2007), which takes the form,

$$(\widehat{\overline{u}}, \widehat{\overline{v}}) = (-\overline{U}_s, -\overline{V}_s). \tag{35}$$

where $\overline{(\cdot)}$ denotes the depth-integrated variable.

2.6. Summary of new terms introduced

The forcing of the wave field on the ocean circulation requires the knowledge of all the fields listed in table 1.

Table 1: List of wave-forcing terms required to force an ocean circulation model solving for the quasi-Eulerian velocity. The J term is a 2D field when the effect of the vertical shear of the quasi-Eulerian current is neglected, as done here. In general J is a 3D forcing field (Ardhuin et al., 2008a). The terms $\tau_{wb,x}$ and $\tau_{wb,y}$ are only used when the wave bottom boundary layer is resolved.

term	type	see eq.
U_s	3D	23
V_s	3D	23
J	2D or 3D	26
$\tau_{aw,x}$	2D	34
$\tau_{aw,y}$	2D	34
$\tau_{oc,x}$	2D	27
$\tau_{oc,y}$	2D	27
$\tau_{wb,x}$	2D	32
$\tau_{wb,y}$	2D	32

Compared to equations for the Lagrangian mean velocity, such as those by Mellor (2003), the amount of data to be transferred is significantly reduced, since the latter form requires, the 3D fields S_{xx}, S_{yy} and S_{xy}, as well as the 3D fields U_s and V_s to correct the velocities before applying the turbulence closure (Walstra et al., 2000). This lower complexity of the quasi-Eulerian equations for the 3D case is contrary to the 2D case, in which seven 2D fields are needed, versus 3 to 5 (if properly dealing with the bottom boundary condition) for the depth-integrated Lagrangian equations. In both cases, for a full consistency of the ocean circulation and wave model, one should also use

the wind stress of the wave model, and the surface flux of turbulent kinetic energy as discussed by Janssen et al. (2004), and a proxy of the breaking wave heights, possibly the wind sea wave height (Rascle et al., 2008).

The wave model can also be used to provide energy fluxes for the surface flux of turbulent kinetic energy (Janssen et al., 2004), or the near-bottom flux of turbulent kinetic energy (TKE) due to bottom friction (Mellor, 2002). For the adiabatic conditions considered here all the stresses τ_{aw}, τ_{wb}, τ_{oc} are zero, together with these fluxes of TKE.

3. Example case of shoaling waves

3.1. Steady wave forcing

The first test of a 3D wave-forced model should be in conditions where the results are known, typically in the absence of dissipative effects in order to compare the solutions given by the difference models with the known solution. So, we will be able to estimate the ability of the different models to simulate the three-dimensional oceanic field flow in presence of waves.

Such a test was proposed by Ardhuin et al. (2008b) with steady monochromatic waves shoaling on a slope without breaking nor bottom friction and for an inviscid fluid. The bottom slopes smoothly from a depth $D = 6$ to $D = 4$ m. Compared to Ardhuin et al. (2008b) the bottom was extend by its symmetric, sloping back down to 6 m, in order to allow periodic boundary conditions if needed (Figure 3). Taking the other parameters unchanged, we consider small incident wave amplitude of 0.12 m and 0.36 m, and a period of 5.24 s and 13 s for numerical simulations with and without vertical mixing. In similar case presented by Ardhuin et al (2008a) the wave amplitude and the wave period are respectively equal to 0.12 m and 5.24 s and the vertical mixing is absent. This was chosen to give a wave steepness $\epsilon_1 = 0.0266$, equal to the maximum bottom slope ϵ_2. A numerical solution is given by Ardhuin et al. (2008b) thanks to the code from Athanassoulis and Belibassakis (1999) which solve the Laplace equation. In this paper, we compare the solutions given by all the theoretical models described above, which have all been implemented in the coupled model. For these shoaling waves the group velocity varies little.

As a result the group velocity varies a little (5.4%) from 4.89 to 4.64 m s^{-1}, due to the fact that the non-dimensional depth kD is close to unity. Because the current is much less than the group speed, the waves propagate with a nearly constant energy flux, resulting in a small increase of wave amplitude,

by 2.7%, in the shallower part of the domain.The Eulerian analysis of that situation was given by Longuet-Higgins (1967), who showed that the mean water level should be 0.32 mm lower in the shallow region, and both studies by Rivero and Arcilla (1995) and Lane et al. (2007), clearly show that there is no other dynamical effect: the Eulerian mean current is steady and simply compensates for the divergence of the wave-induced mass transport. Because the relative variation in phase speed is more important, from 6.54 to 5.65 $\mathrm{m\ s^{-1}}$, it produces a strong divergence of the Stokes drift, which accelerates in shallow water. The quasi-Eulerian velocity is irrotational, thus nearly depth-uniform, and compensates the Stokes drift divergence by a strong convergence. This situation is a stationary solution.

3.2. Some details about the numerical simulations

The numerical simulation are realized thanks to a new wave-current model called MARS-WWATCH. Its a modelling system that combines the WAVEWATCH III$^{\mathrm{TM}}$ numerical wave model (Tolman, 2008, 2009) and the MARS3D ocean circulation model (Lazure and Dumas, 2008), coupled by the automatic coupler PALM (Buis et al., 2008). This allows a two-way coupling between the wave and circulation models. Within the scope of this study, in order to simplify comparisons with previous work, disabled the feedback from the flow to the waves. A depth-integrated (2D) version of this new coupled model based on the Phillips (1977) equations was also developped and validated with the data of the nearshore NSTS experiment (Bennis et al., 2010).

In the present study, the numerical simulations are non-stationary: starting from rest, a steady wave field propagates from left to right, quickly filling up the entire domain, and then becoming stationary. The monochromatic wave amplitude of 0.12 m translates in a significant wave height H_s of 0.34 m in the case of random waves with the same energy. We will also test the models with a higher amplitude of 0.36 m, i.e. $H_s = 1.02$ m, still far from the breaking limit in 4 m depth.

Our MARS3D model setting uses 100 sigma levels[5] regularly spaced, 5 active points in the y direction and 78 active points in the x direction. The time step was set to 0.05 s for the $H_s = 1.02$ m tests (and 1 s for $H_s = 0.34$ m).

[5]The vertical resolution is specific to this study and the ARB08 model can be used with coarser vertical resolution.

The ARB08 model has been tested with one active point in y-direction and the time step was set to 1 s for all numerical simulations. For the sake of simplicity, the wave model time step is taken equal to the flow model time step and they are coupled at each time step. The first tests are done without any bottom friction nor internal mixing. The MARS3D model uses open boundary conditions for the lateral boundaries (East and West).

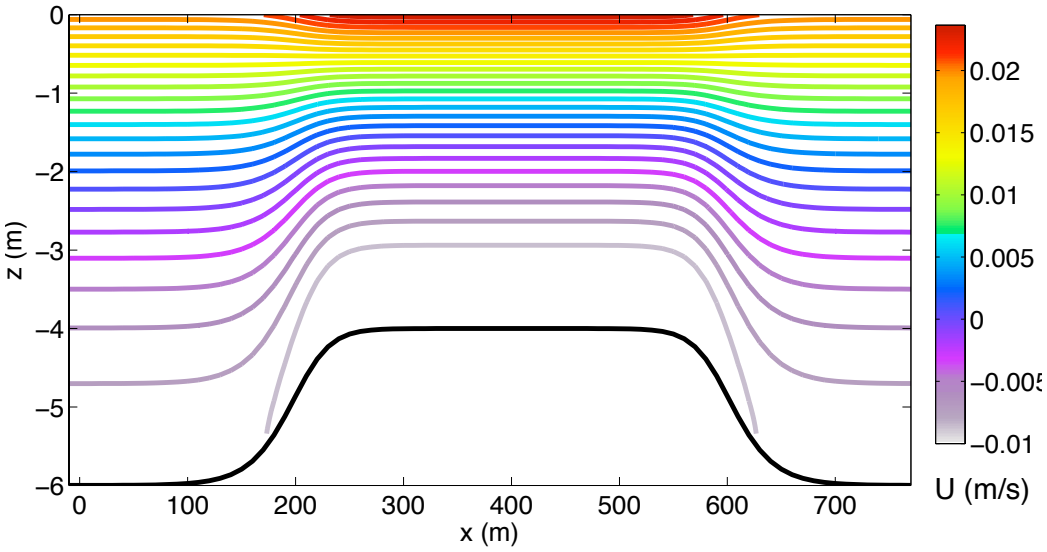

Figure 3: Lagrangian velocity U for the inviscid sloping bottom case with $H_s = 1.02$ m, $T = 5.24$ s and without mixing, obtained from the quasi-Eulerian analysis as $U = \widehat{u} + U_s$. Contours are equally spaced from -0.01 to 0.025 m s^{-1}. The thick black line is the bottom elevation.

3.3. The M03 model (Mellor, 2003)

We now solve for the equations by Mellor (2003) (equation (10)), which, if correct, should lead to the steady Lagrangian velocity shown in Figure 3. First, we validated our implementation of this model with the results given by the temporal integration of equation (10) with $W = 0$ (the vertical velocity is negligible for the considered time) that correspond to the following expression,

$$U(t) = \int_0^t \left(-U \frac{\partial U}{\partial x} + \frac{F}{D} \right) dt. \tag{36}$$

In our case the wave field is steady after about 5 minutes, which correspond to the time needed for the waves to cross the domain. On the up-slope the steady forcing produces a surface force F in the direction of wave propagation, and a reverse force at the bottom. Thus the Lagrangian velocity U increases linearly until the advection becomes significant. The surface and bottom accelerations produced by the coupled model are identical to the simplified equation (36), which validates our implementation of M03 in the coupled model (see Figure 4). Figure 5 also shows that the initial velocity evolution is simply given by the time integration of the forcing term $\dfrac{F}{D}$, with later saturation due to the lateral advection. The red line with circles correspond to the lagrangian velocity computed by MARS-WWATCH. This simple interpretation of the MARS-WWATCH solution, in relation to the forcing F shows that the M03 equations were correctly implemented.

The surface velocity is associated to a counter-current below (Figure 4), producing a circulation pattern very different from the known correct solution (Figure 3). In spite of the small bottom slope and wave steepness, the resulting velocity reaches 17 cm s^{-1} in only 15 minutes, which is about 10 times the correct solution shown in Figure 3. Further, if the model is integrated for a longer time, the region of positive acceleration on the up-slope meets the region of negative acceleration on the down-slope, resulting in large vertical velocities and further strange model adjustments.

As shown by Ardhuin et al. (2008a), the force term F is proportional to $gD\varepsilon_1^2\varepsilon_2$, where ε_1 is the wave steepness, ε_2 is the bottom slope. For the bottom shape and wave period chosen here, the maximum value of F is $0.29gD\varepsilon_1^2\varepsilon_2$. Obviously, the depth dependence of F plays an important role and F becomes depth-uniform for $kD \to 0$, so that one may expect that the problem could vanish in shallow water.

Unfortunately, in practice, the velocity at which the current first stabilizes (here after 15 minutes), is *independent* of ε_2, provided that the change in water depth remains the same. If the bottom topography is stretched by a factor $1/\alpha$ in the x direction, the slope increases by a factor α and the change advection compensates the local increase of F. Mathematically, equation (10) follows a Froude scaling: when x is replaced by $x' = \alpha x$ and t by $t' = \alpha^2 t$, the equation is unchanged if $F' = \alpha F$, and thus $U(x', t') = U(x, t)$.

As a result, for any wave field approaching the shore from deep water, even on a very gently sloping continental shelf, there will be a very large spurious onshore velocity at the surface. Based on the present case, this

velocity should be at least of the order of 10 to 20 times the Stokes drift. This momentum is generated where $kD \sim 1$, and self-advects onshore.

Obviously, some realistic mixing will reduce this effect. Using a realistic constant eddy viscosity of 2.8×10^{-3} m^2.s^{-1} only reduces the current by about a factor 2 to 3 (see Table 2). This factor depends on the wave amplitude since the introduction of viscosity breaks the Froude scaling.

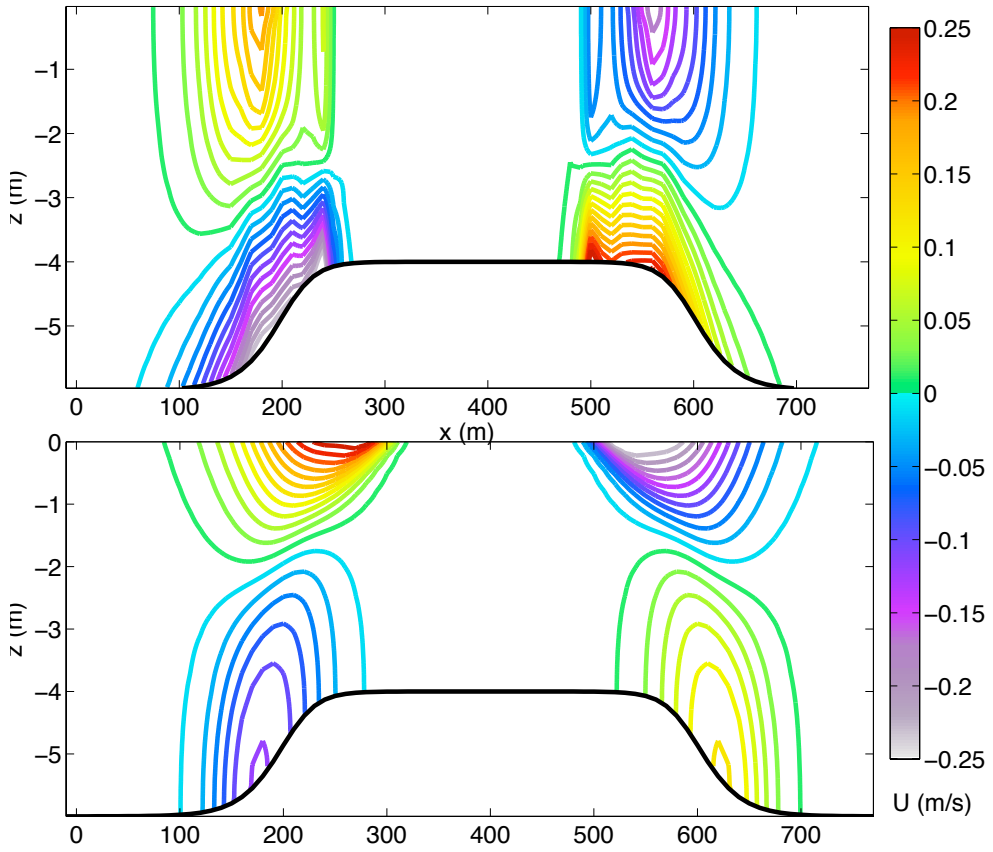

Figure 4: **M03 model**: Lagrangian velocity U solution of the coupled model after 15 minutes of integration (top panel) and simple integration in time of $F/D - U\partial U/\partial x$ (bottom panel). The thick black line is the bottom elevation. $H_s = 1.02\,\mathrm{m}$, $T = 5.26\,\mathrm{s}$, $K_z = 0\,\mathrm{m}^2.\mathrm{s}^{-1}$.

3.4. The M08 model (Mellor, 2008)

After acknowledging the problem in the M03 equations, Mellor (2003) proposed a new set of equations. Unfortunately he did not keep the correct

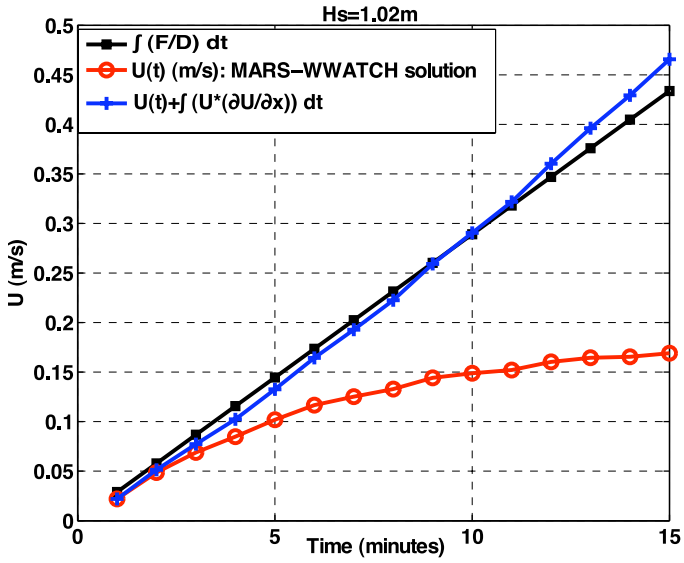

Figure 5: Lagrangian velocity $U(t)$ at the surface $z = \widehat{\eta}$, at the position x =200 m and without vertical mixing. The MARS-WWATCH solution without advection terms (blue line) is compared to the linear trend given by a constant acceleration F/D, and the numerical integration of F/D (black line). Red line: the entire solution computed by MARS-WWATCH. $H_s = 1.02\,\mathrm{m}$, $T = 5.26\,\mathrm{s}$, $K_z = 0\,\mathrm{m}^2.\mathrm{s}^{-1}$.

Table 2: **Model results for the M03 model**: Surface velocity at x =200 m for different model settings. The settings corresponding to the test in Ardhuin et al. (2008b) are given in the second line $H_s = 0.34\,\mathrm{m}$, $T = 5.6\,\mathrm{s}$, K_z=0 $\mathrm{m}^2\ \mathrm{s}^{-1}$. The surface velocity values are written for $T = 900\,\mathrm{s}$ where $H_s = 1.02\,\mathrm{m}$ and for $T = 2700\,\mathrm{s}$ where $H_s = 0.34\,\mathrm{m}$.

H_s (m)	T_p (s)	K_z ($\mathrm{m}^2.\mathrm{s}^{-1}$)	resulting U ($\mathrm{m.s}^{-1}$)
1.02	5.6	0	0.1698
0.34	5.6	0	0.0537
0.34	13	0	0.0110
1.02	5.6	$2.8.10^{-3}$	0.1094
0.34	5.6	$2.8.10^{-3}$	0.0185
0.34	13	$2.8.10^{-3}$	0.0026

part in M03 (before the approximation using Airy theory), and, as discussed above, he produced another inconsistent set of equations. Both M03 and

M08 model are similar in the sense that they are based on the same vertical coordinate ς and apply to the total momentum U, but with a different forcing F (see section 1.2). We warn the reader that the result of these equations should not be compared directly with results of other equations for the quasi-Eulerian momentum $\widehat{u}$, such as given by Uchiyama et al. (2010), but rather that U should be compared with $\widehat{u} + U_s$.

Here we investigate the consequence of the inconsistency in the M08 equations, using the same test case and numerical set-up used for M03. The discontinuity of the forcing F, due to the E_D term generated some numerical problems when we used a fine vertical resolution (here from 4 to 6 cm). Indeed, the author of the M08 model, explain in the paper that the E_D term for finite difference scheme must be only applied in the top layer which has a thickness equal to δz without restrictions for δz such as

$$\frac{\partial E_D}{\partial x} = \frac{1}{\delta z}\frac{\partial (E/2)}{\partial x}. \tag{37}$$

For 4cm $\leq \delta z \leq$ 6cm, strongly oscillations are generated at the surface (Figure 6: black line). These oscillations are absent at depths larger than 0.8 m, consistent with the zero values of F below the surface. We note that the vertical shear in the exact solution for $U = \widehat{u} + U_s$, which comes from U_s, in not reproduced by M08. One solution for this problem could be to diffuse the E_D term over the vertical. A realistic constant viscosity $K_z = 2.8.10^{-3}$ m^2 s^{-1} removes the oscillations by diffusing the positive E_D term over the vertical. Yet E_D is a momentum source that produces velocities one order of magnitude larger than the Stokes drift U_s. The velocities given by M08 with a realistic mixing are thus comparable in magnitude with those given by M03 without mixing, most pronounced for waves in intermediate shallow water (Table 3). Moreover, the flow computed by M08 with mixing and therefore without "numerical problem" due to δz (Figure 7) is similar to the one given by the M03 model (Figure 4) with a bipolar structure that differs from the reference flow (Figure 5). Also the wave-induced set down in this case is 50% too large (Figure 8). Although these problems may be secondary in the surf zone (Kumar et al., personal communication), they are likely to be dominant on the shelf outside of the surf zone.

3.5. Results with the glm2 equations

In this section, we test the *glm*2 model on the same test case as previously. This model based on equations (18) and (19) has been implemented

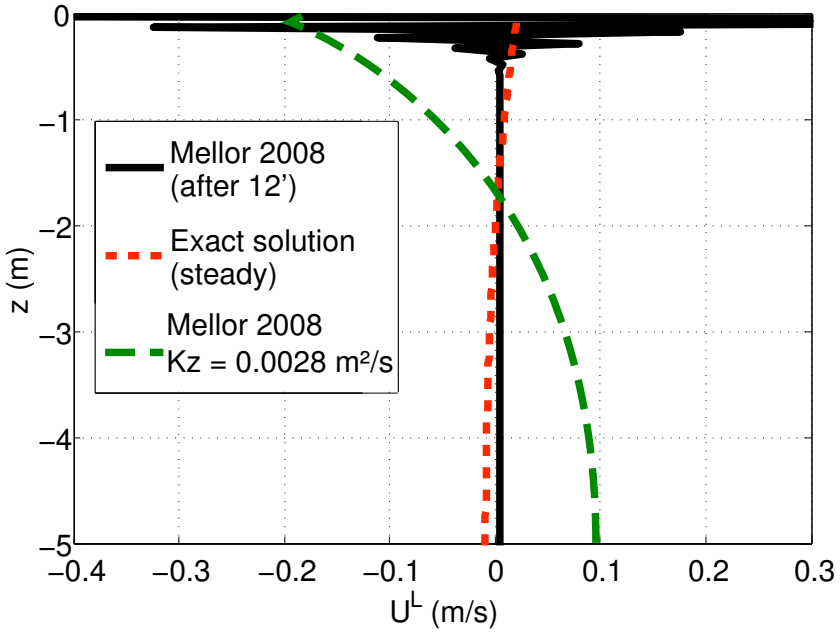

Figure 6: Comparison of vertical profiles of the lagrangian velocity U given by different models at $x = 200\,\mathrm{m}$: M08 without mixing (solid black line), M08 with mixing (dashed green line), exact solution (dashed red line). The wave parameters are $H_s = 1.02\,\mathrm{m}$ and $T = 5.26\,\mathrm{s}$. All profiles are plotted after six minutes of time integration. The x-axis was clipped, and the maximum velocities with M08 reached 0.8 m s^{-1}.

in the coupled model that solve now the quasi-Eulerian velocity (Lagrangian velocity minus Stokes velocity). In order to compare with the reference solution (see Figure 3) which correspond to the Lagrangian velocity, we add the Stokes drift, computed by the coupled model, to the quasi-Eulerian velocity from the coupled model.

The *glm*2 equations give a quasi-Eulerian current solution $\widehat{u}$, and thus differs from the M08 and M03 models. The dynamic effect of the waves is conveyed by dynamic forcing terms (see terms A_1, A_2, B_1, B_2 in equations (18) and (19)) and an equivalent mass source at the surface (eq. (22)). The depth-integration of the ARB08 model gives the Smith model (Smith, 2006) and the sea surface elevation computed by the coupled model with ARB08 is coherent with the one given by Longuet-Higgins (Figure 8). The quasi-Eulerian current is nearly depth-uniform as expected (Figure 10). As a result, the Lagrangian current given by the ARB08 model (Figure 9) is similar to

Table 3: **Model results with Mellor (2008b):** Surface velocity at x =200 m for different model settings. The settings corresponding to the test in Ardhuin et al. (2008b) are given in the second line. The surface velocity values are written for the time $t = 900$ s except for the case without mixing ($t = 360$ s).

H_s(m)	T_p(s)	K_z (m^2 s^{-1})	U (m s^{-1})
1.02	5.6	0	0.6116
0.34	5.6	0	0.2127
0.34	13	0	0.3164
1.02	5.6	$2.8.10^{-3}$	-0.1594
0.34	5.6	$2.8.10^{-3}$	-0.0256
0.34	13	$2.8.10^{-3}$	-0.0007

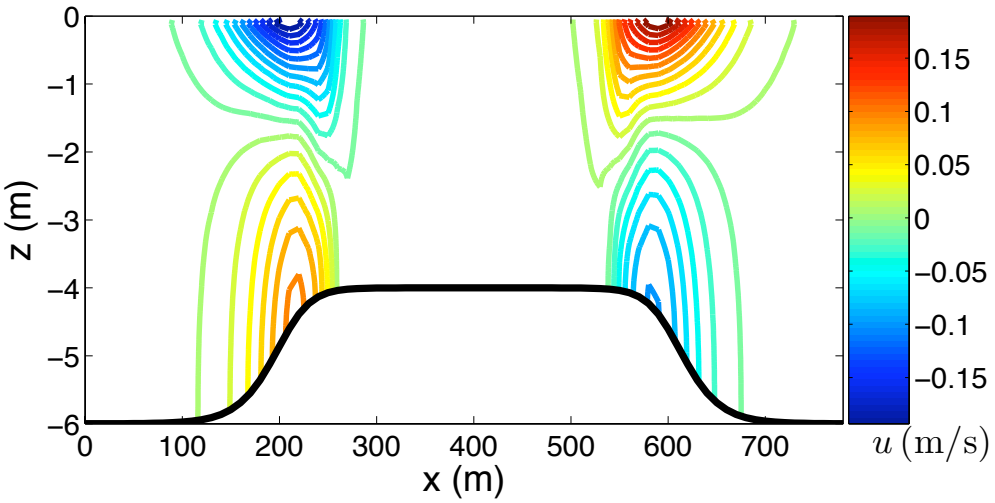

Figure 7: **M08 model**: Lagrangian velocity U(m/s) of the coupled model after 15 minutes of integration with $H_s = 1.02$ m, $T = 5.24$ s, $K_z = 2.8.10^{-3}$ m^2.s^{-1}. The thick black line is the bottom elevation.

the reference current (Figure 3). The flow structure and the intensity of the flow are within a fraction of a percent.

The implementation of the ARB08 model in the coupled model is validated by these results and we can conclude that the ARB08 model correctly simulates for this case the three-dimensional flow in presence of waves.

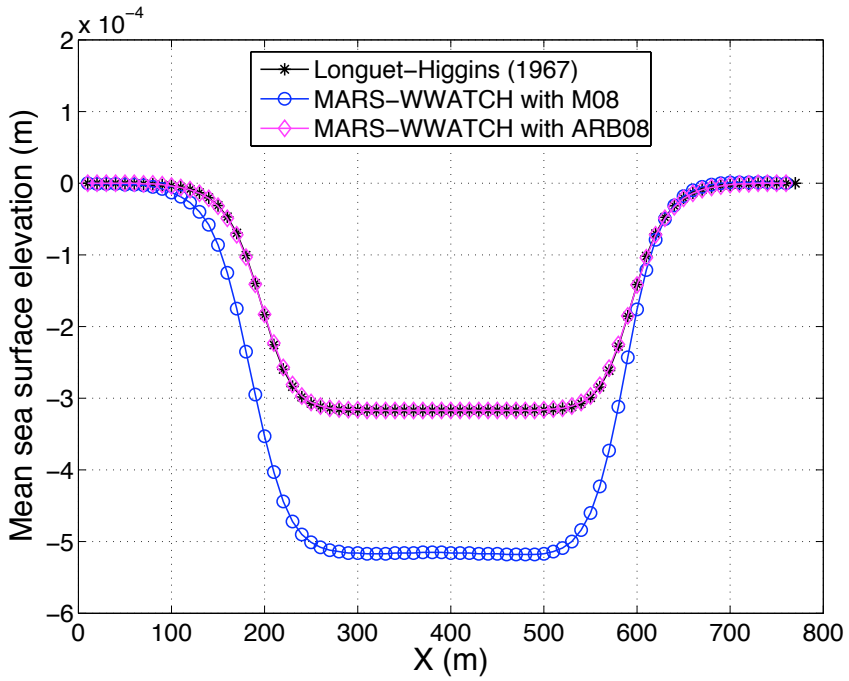

Figure 8: **Mean sea surface elevation**: comparison between the MARS-WWATCH solution with M08 (blue line with circle) and MARS-WWATCH solution with ARB08 (pink line with diamond) and the solution given by Longuet-Higgins (1967) (black line with asterisk). $H_s = 0.34$ m, $T = 5.24$ s.

4. Conclusion

It was demonstrated here that equations for the three-dimensional wave-forced circulation that are formulated in terms of the Lagrangian mean velocity (total momentum) and use analytical functions of the local wave field and topography produce spurious velocities that can be very large. This result was anticipated by Ardhuin et al. (2008b) who showed that the vertical flux of momentum is a non-local function of the water depth that may be estimated from non-local evanescent wave modes. The magnitude of the problem is revealed by the present study. In particular, the equations proposed by Mellor (2003) et Mellor (2008) can produce solutions with order of magnitude errors in adiabatic conditions, and still very large errors when a reasonable vertical mixing is included. These error may become negligible in

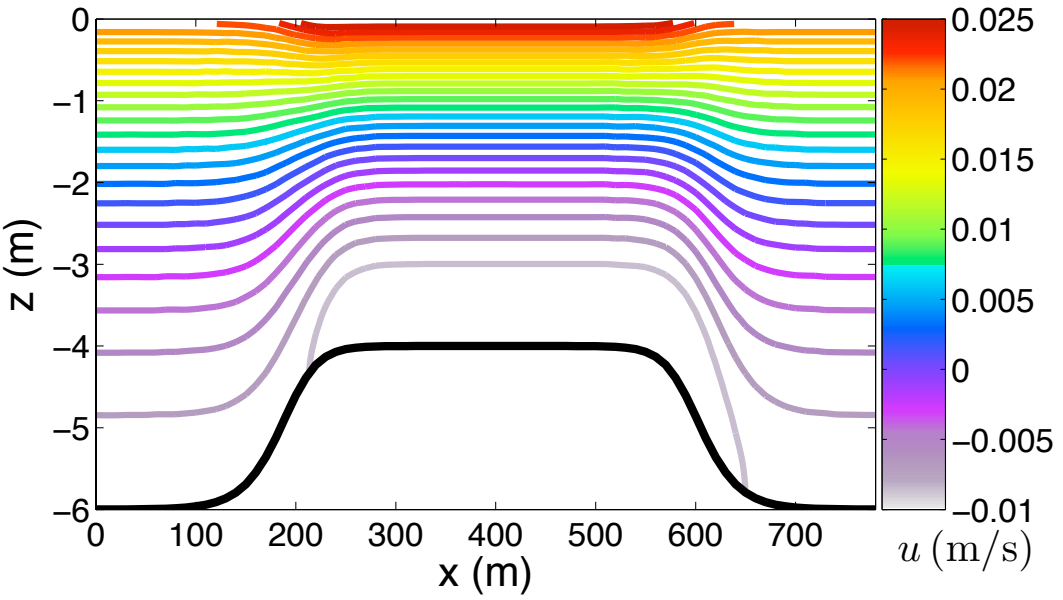

Figure 9: **ABR08 model**: Lagrangian velocity U(m/s) of the coupled model when a steady state is reached and with $H_s = 1.02$ m, $T = 5.24$ s and $K_z = 0\,\mathrm{m}^2.\mathrm{s}^{-1}$. The thick black line is the bottom elevation.

the surf zone, and they still likely plays a big part in the differences in vertical velocity profiles reported by Haas and Warner (2009), when comparing a version of ROMS solving the Mellor (2003) equations with SHORECIRC (see their figure 4). We also wish to point out another common source of differences between model results. Some models, like SHORCIRC solve for the quasi-Eulerian mean velocity $U - U_s$ while the other model solves for the Lagrangian mean velocity U. The difference between the two is the Stokes drift, which can be very large in the surf zone, up to 30% of the wave phase speed (Ardhuin et al., 2008b).

From the present model results, we conclude that there is no acceptable short-cut to a three-dimensional equation for the Lagrangian velocity U: the only possibility would be to solve for the wave motion to first order in the bottom slope. This requires a model of the kind developed by Athanassoulis and Belibassakis (1999) and Gerosthathis et al. (2005), with at least 10 vertical modes. Given the large effort required for a 4 by 4 km region with only 3

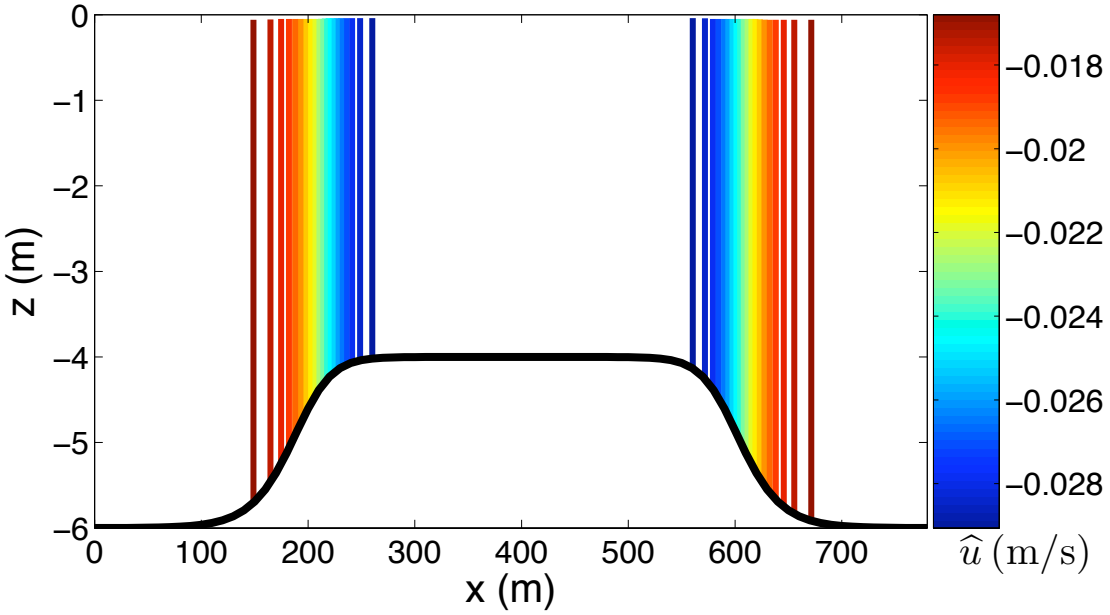

Figure 10: **ABR08 model**: Quasi-Eulerian velocity $\widehat{u}$(m/s) of the coupled model when a steady state is reached and with $H_s = 1.02$ m, $T = 5.24$ s and $K_z = 0\,\mathrm{m}^2.\mathrm{s}^{-1}$. The thick black line is the bottom elevation.

modes (Magne et al., 2007), this is hardly a practical solution. The only practical solution is thus the use of a momentum equation for the quasi-Eulerian velocity, such as proposed by McWilliams et al. (2004), Newberger and Allen (2007b), or Ardhuin et al. (2008a). This approach has been applied to surf zone problems by Rascle (2007) and Uchiyama et al. (2010).

Acknowledgments

The Authors express their gratitude to P. Marsaleix for his proof-reading and advice. A-C. B. acknowledges the support of a post-doctoral grant from INSU and grant ANR-BLAN-08-0330-01, and F.A. is supported by a FP7-ERC grant 240009 "IOWAGA" and the NOPP program through ONR grant N00014-10-1-0383.

Appendix A. glm2 equations in sigma coordinates : Momentum, mass, tracer conservation

Let (x, y, z, t) denote the cartesian coordinate system and $(x^\star, y^\star, \varsigma, t^\star)$ the sigma coordinate system.

$$\begin{aligned}\frac{\partial \widehat{u}}{\partial t^\star} &+ \widehat{u}\frac{\partial \widehat{u}}{\partial x^\star} + \widehat{v}\frac{\partial \widehat{u}}{\partial y^\star} + \widehat{\mathcal{W}}\frac{\partial \widehat{u}}{\partial \varsigma} - f\widehat{v} + \frac{1}{\rho}\left(\frac{\partial p^H}{\partial x^\star} + \frac{\partial p^H}{\partial \varsigma}\cdot\frac{\partial \varsigma}{\partial x}\right) \\ &= \left[f + \left(\frac{\partial \widehat{v}}{\partial x^\star} + \frac{\partial \widehat{v}}{\partial \varsigma}\cdot\frac{\partial \varsigma}{\partial x}\right)\right] V_s - \left(\frac{\partial \widehat{u}}{\partial y^\star} + \frac{\partial \widehat{u}}{\partial \varsigma}\cdot\frac{\partial \varsigma}{\partial y}\right) V_s \\ &\quad -\frac{W_s}{D}\cdot\frac{\partial \widehat{u}}{\partial \varsigma} - \frac{\partial J}{\partial x^\star} - \frac{\partial J}{\partial \varsigma}\cdot\frac{\partial \varsigma}{\partial x} + \widehat{F}_{d,x} + \widehat{F}_{m,x} + \widehat{F}_{b,x}, \qquad \text{(A.1)}\end{aligned}$$

and

$$\begin{aligned}\frac{\partial \widehat{v}}{\partial t^\star} &+ \widehat{u}\frac{\partial \widehat{v}}{\partial x^\star} + \widehat{v}\frac{\partial \widehat{v}}{\partial y^\star} + \widehat{\mathcal{W}}\frac{\partial \widehat{v}}{\partial \varsigma} + f\widehat{u} + \frac{1}{\rho}\left(\frac{\partial p^H}{\partial y^\star} + \frac{\partial p^H}{\partial \varsigma}\cdot\frac{\partial \varsigma}{\partial y}\right) \\ &= -\left[f + \left(\frac{\partial \widehat{v}}{\partial x^\star} + \frac{\partial \widehat{v}}{\partial \varsigma}\cdot\frac{\partial \varsigma}{\partial x}\right)\right] U_s + \left(\frac{\partial \widehat{u}}{\partial y^\star} + \frac{\partial \widehat{u}}{\partial \varsigma}\cdot\frac{\partial \varsigma}{\partial y}\right) U_s \\ &\quad -\frac{W_s}{D}\cdot\frac{\partial \widehat{v}}{\partial \varsigma} - \frac{\partial J}{\partial y^\star} - \frac{\partial J}{\partial \varsigma}\cdot\frac{\partial \varsigma}{\partial y} + \widehat{F}_{d,y} + \widehat{F}_{m,y} + \widehat{F}_{b,y}. \qquad \text{(A.2)}\end{aligned}$$

where

- $\varsigma = \dfrac{z - \widehat{\eta}}{D}$ is the sigma coordinate with $\widehat{\eta}$ the mean elevation, h the bottom depth and $D = \widehat{\eta} + h$ the mean water column depth,
- $\widehat{\mathcal{W}} = \left(\dfrac{\partial \varsigma}{\partial t} + \widehat{u}\dfrac{\partial \varsigma}{\partial x} + \widehat{v}\dfrac{\partial \varsigma}{\partial y} + \dfrac{\widehat{w}}{D}\right)$,
- $\dfrac{\partial \varsigma}{\partial x} = -\dfrac{1}{D}\cdot\dfrac{\partial \widehat{\eta}}{\partial x} - \dfrac{\varsigma}{D}\cdot\dfrac{\partial D}{\partial x}$,
- $\dfrac{\partial \varsigma}{\partial y} = -\dfrac{1}{D}\cdot\dfrac{\partial \widehat{\eta}}{\partial y} - \dfrac{\varsigma}{D}\cdot\dfrac{\partial D}{\partial y}$,
- $\dfrac{\partial \varsigma}{\partial t} = -\dfrac{(\varsigma + 1)}{D}\cdot\dfrac{\partial \widehat{\eta}}{\partial t}$,

- $(\widehat{F}_{b,x}, \widehat{F}_{b,y})$ are only used when the wave bottom boundary layer is resolved.

The depth-integrated continuity equation becomes

$$\frac{\partial \widehat{\eta}}{\partial t} + \frac{\partial \left[D(\overline{\widehat{u}} + \overline{U}_s) \right]}{\partial x^\star} + \frac{\partial \left[D(\overline{\widehat{v}} + \overline{V}_s) \right]}{\partial y^\star} = 0. \tag{A.3}$$

where $\overline{(\cdot)}$ denotes depth-integrated variable.

The evolution of a conservative passive tracer concentration $\mathcal{C}$ is,

$$\frac{\partial (D\mathcal{C})}{\partial t^\star} + \frac{\partial [D(\widehat{u} + U_s)\mathcal{C}]}{\partial x^\star} + \frac{\partial [D(\widehat{v} + V_s)\mathcal{C}]}{\partial y^\star} + \frac{\partial (\omega \mathcal{C})}{\partial \varsigma} = 0. \tag{A.4}$$

where

$$\omega = \widehat{w} + W_s + D\frac{\partial \varsigma}{\partial t} + D(\widehat{u} + U_s)\frac{\partial \varsigma}{\partial x} + D(\widehat{v} + V_s)\frac{\partial \varsigma}{\partial y}. \tag{A.5}$$

Appendix B. Flux formulations of the quasi-Eulerian *glm2* equations in sigma coordinates : Momentum, mass, tracer conservation

$$\begin{aligned} \frac{\partial D\widehat{u}}{\partial t^\star} \; + \; & \frac{\partial [D(\widehat{u} + U_s)\widehat{u}]}{\partial x^\star} + \frac{\partial [D(\widehat{v} + V_s)\widehat{u}]}{\partial y^\star} + \frac{\partial (\omega \widehat{u})}{\partial \varsigma} - f\widehat{v} + \frac{1}{\rho} \cdot \left(\frac{\partial p^H}{\partial x^\star} + \frac{\partial p^H}{\partial \varsigma}\frac{\partial \varsigma}{\partial x} \right) \\ = \; & U_s D \left(\frac{\partial \widehat{u}}{\partial x^\star} + \frac{\partial \widehat{u}}{\partial \varsigma}\frac{\partial \varsigma}{\partial x} \right) + \left(f + D\frac{\partial \widehat{v}}{\partial x^\star} + D\frac{\partial \widehat{v}}{\partial \varsigma}\frac{\partial \varsigma}{\partial x} \right) V_s - \frac{\partial J}{\partial x^\star} - \frac{\partial J}{\partial \varsigma}\frac{\partial \varsigma}{\partial x} \\ & + \widehat{F}_{d,x} + \widehat{F}_{m,x} + \widehat{F}_{b,x}, \end{aligned} \tag{B.1}$$

and

$$\begin{aligned} \frac{\partial D\widehat{v}}{\partial t^\star} \; + \; & \frac{\partial [D(\widehat{u} + U_s)\widehat{v}]}{\partial x^\star} + \frac{\partial [D(\widehat{v} + V_s)\widehat{v}]}{\partial y^\star} + \frac{\partial (\omega \widehat{v})}{\partial \varsigma} + f\widehat{u} + \frac{1}{\rho} \cdot \left(\frac{\partial p^H}{\partial y^\star} + \frac{\partial p^H}{\partial \varsigma}\frac{\partial \varsigma}{\partial y} \right) \\ = \; & V_s D \left(\frac{\partial \widehat{v}}{\partial y^\star} + \frac{\partial \widehat{v}}{\partial \varsigma}\frac{\partial \varsigma}{\partial y} \right) - \left(f - D\frac{\partial \widehat{u}}{\partial y^\star} - D\frac{\partial \widehat{u}}{\partial \varsigma}\frac{\partial \varsigma}{\partial y} \right) U_s - \frac{\partial J}{\partial y^\star} - \frac{\partial J}{\partial \varsigma}\frac{\partial \varsigma}{\partial y} \\ & + \widehat{F}_{d,y} + \widehat{F}_{m,y} + \widehat{F}_{b,y}. \end{aligned} \tag{B.2}$$

where ω is defined by equation (A.5) and $(\widehat{F}_{b,x}, \widehat{F}_{b,y})$ are only used when the wave bottom boundary layer is resolved.

The continuity equation becomes

$$\frac{\partial \widehat{\eta}}{\partial t} + \frac{\partial \left[D(\widehat{u} + U_s)\right]}{\partial x^\star} + \frac{\partial \left[D(\widehat{v} + V_s)\right]}{\partial y^\star} + \frac{\partial \omega}{\partial \varsigma} = 0, \tag{B.3}$$

and the evolution of a conservative passive tracer concentration $\mathcal{C}$ is defined by equation (A.4).

We notice that only the horizontal components of stokes drift (U_s, V_s) must be known with this formulation. The W_s depending terms are removed.

Appendix C. Explicit form of random wave forcing terms for the quasi-Eulerian velocity

For random waves, eq. (23) becomes

$$(U_s, V_s) = \int \sigma k(\cos\theta, \sin\theta) E(f,\theta) \frac{\cosh(2kz + 2kh)}{\sinh^2(kD)} \mathrm{d}f\mathrm{d}\theta, \tag{C.1}$$

where $E(f,\theta)$ is the spectral density of the surface wave elevation variance, usually known as the wave spectrum, the state variable of most numerical wave models, and the wave-induced pressure term becomes,

$$J = \int g \frac{kE(f,\theta)}{\sinh 2kD} \mathrm{d}f\mathrm{d}\theta. \tag{C.2}$$

Appendix D. Forcing terms for the Lagrangian mean velocity

The horizontal and vertical radiation stresses in ς coordinate take the form,

$$F_{uu} = -\frac{\partial S_{xx}}{\partial x} = -\frac{\partial}{\partial x}\left(\overline{D\widetilde{u}^2 + \widetilde{p}\frac{\partial \widetilde{s}}{\partial \varsigma}}\right). \tag{D.1}$$

Using Airy theory, S_{xx} is given by,

$$\begin{aligned} S_{xx} &= \int kDE(f,\theta) \left[\cos^2\theta F_{CS}F_{CC} \right. \\ &\quad \left. + (F_{CS}F_{CC} - F_{SS}F_{CS})\right] \mathrm{d}f\mathrm{d}\theta, \end{aligned} \tag{D.2}$$

and the vertical profile function F_{CS} changes with f and is defined by

$$F_{CS} = \frac{\cosh\left[kD(\,1+\varsigma\,)\right]}{\sinh\left(kD\right)}, \tag{D.3}$$

with similar definitions for F_{SS} (respectively F_{CC}), replacing cosh in the numerator (respectively sinh in the denominator) by sinh (respectively cosh).

The horizontal force that is given by the vertical divergence of S_{x3} is

$$F_{p3} = -\frac{\partial S_{x3}}{\partial \varsigma} = \frac{\partial}{\partial \varsigma}\left(\overline{\widetilde{p}\partial\widetilde{s}/\partial x}\right). \tag{D.4}$$

In this case, Airy theory is insufficient for a consistent approximation. Yet Mellor (2003) still used Airy theory, thus producing the erroneous expression,

$$\begin{aligned} S_{x3} &= -\int (F_{CC} - F_{SS}) \\ &\quad \times \left[E(f,\theta)\frac{\partial F_{SS}}{\partial x} + \frac{F_{SS}}{2}\frac{\partial E(f,\theta)}{\partial x}\right] \mathrm{d}f\mathrm{d}\theta. \end{aligned} \tag{D.5}$$

References

Andrews, D. G., McIntyre, M. E., 1978. An exact theory of nonlinear waves on a Lagrangian-mean flow. J. Fluid Mech. 89, 609–646.

Ardhuin, F., Chapron, B., Elfouhaily, T., 2004. Waves and the air-sea momentum budget, implications for ocean circulation modelling. J. Phys. Oceanogr. 34, 1741–1755.
URL http://www.shom.fr/fr_page/fr_act_oceano/vagues/PLUS/PUBLIS/

Ardhuin, F., Herbers, T. H. C., Jessen, P. F., O'Reilly, W. C., 2003a. Swell transformation across the continental shelf. part II: validation of a spectral energy balance equation. J. Phys. Oceanogr. 33, 1940–1953.
URL http://ams.allenpress.com/archive/1520-0485/33/9/pdf/i1520-0485-33-9-1940.pdf

Ardhuin, F., Jenkins, A. D., Belibassakis, K., 2008a. Commentary on 'the three-dimensional current and surface wave equations' by George Mellor. J. Phys. Oceanogr. 38, 1340–1349.
URL http://ams.allenpress.com/archive/1520-0485/38/6/pdf/i1520-0485-38-6-1340.pdf

Ardhuin, F., Marié, L., Rascle, N., Forget, P., Roland, A., 2009a. Observation and estimation of Lagrangian, Stokes and Eulerian currents induced by wind and waves at the sea surface. J. Phys. Oceanogr. 39 (11), 2820–2838.
URL http://ams.allenpress.com/archive/2541-2558/39/11/pdf/i1520-0485-39-11-2820.pdf

Ardhuin, F., O'Reilly, W. C., Herbers, T. H. C., Jessen, P. F., 2003b. Swell transformation across the continental shelf. part I: Attenuation and directional broadening. J. Phys. Oceanogr. 33, 1921–1939.

Ardhuin, F., Rascle, N., Belibassakis, K. A., 2008b. Explicit wave-averaged primitive equations using a generalized Lagrangian mean. Ocean Modelling 20, 35–60.

Ardhuin, F., Rogers, E., Babanin, A., Filipot, J.-F., Magne, R., Roland, A., van der Westhuysen, A., Queffeulou, P., Lefevre, J.-M., Aouf, L., Collard, F., 2009b. Semi-empirical dissipation source functions for wind-wave models: part i, definition, calibration and validation. J. Phys. Oceanogr. accepted for publication, –.
URL http://hal.archives-ouvertes.fr/hal-00201380/

Athanassoulis, G. A., Belibassakis, K. A., 1999. A consistent coupled-mode theory for the propagation of small amplitude water waves over variable bathymetry regions. J. Fluid Mech. 389, 275–301.

Bennis, A.-C., Ardhuin, F., Odaka, T., 2010. Modélisation couplée vagues-courant : développements avec MARS3D et WAVEWATCH III. In: Actes des XIèmes journées Génie côtier-Génie civil, Les Sables d'Olonnes. Centre Français du Littoral, pp. 17–24.

Blumberg, A. F., Mellor, G. L., 1987. A description of a three-dimensional coastal ocean model. In: Heaps, N. S. (Ed.), Three Dimensional Coastal Ocean Models. American Geophysical Union, pages 1–16.

Buis, S., Piacentini, A., Déclat, D., 2008. PALM: A computational framework for assembling high performance computing applications. Concurrency Computat.: Pract. Exper. 18 (2), 247–262.

Craig, P. D., Banner, M. L., 1994. Modeling wave-enhanced turbulence in the ocean surface layer. J. Phys. Oceanogr. 24, 2546–2559.
URL http://ams.allenpress.com/archive/1520-0485/24/12/pdf/i1520-0485-24-12-2546.pdf

Dolata, L. F., Rosenthal, W., 1984. Wave setup and wave-induced currents in coastal zones. J. Geophys. Res. 89 (C2), 1973–1982.

Garrett, C., 1976. Generation of Langmuir circulations by surface waves - a feedback mechanism. J. Mar. Res. 34, 117–130.

Gerosthathis, T., Belibassakis, K. A., Athanassoulis, G., 2005. Coupled-mode, phase-resolving model for the transformation of wave spectrum over steep 3d topography. a parallel-architecture implementation. In: Proceedings of OMAE 2005 24th International Conference on Offshore Mechanics and Arctic Engineering, June 12–17, 2005 - Halkidiki, Greece. ASME, New York, N.Y., pp. OMAE2005–67075.

Groeneweg, J., 1999. Wave-current interactions in a generalized Lagrangian mean formulation. Ph.D. thesis, Delft University of Technology, The Netherlands.

Groeneweg, J., Klopman, G., 1998. Changes in the mean velocity profiles in the combined wave-current motion described in GLM formulation. J. Fluid Mech. 370, 271–296.

Haas, K. A., Svendsen, I. A., Haller, M. C., Zhao, Q., 2003. Quasi-three-dimensional modeling of rip current systems. J. Geophys. Res. 108 (C7), 3217, doi:10.1029/2002JC001355.

Haas, K. A., Warner, J. C., 2009. Comparing a quasi-3d to a full 3d nearshore circulation model: SHORECIRC and ROMS. Ocean Modelling 39, 91–103.

Hasselmann, K., 1971. On the mass and momentum transfer between short gravity waves and larger-scale motions. J. Fluid Mech. 4, 189–205.

Janssen, P. A. E. M., Saetra, O., Wettre, C., Hersbach, H., 2004. Impact of the sea state on the atmosphere and ocean. Annales Hydrographiques 6e série, vol. 3 (772), 3–1–3–23.

Jenkins, A. D., 1989. The use of a wave prediction model for driving a near-surface current model. Deut. Hydrogr. Z. 42, 133–149.

Lane, E. M., Restrepo, J. M., McWilliams, J. C., 2007. Wave-current interaction: A comparison of radiation-stress and vortex-force representations. J. Phys. Oceanogr. 37, 1122–1141.

Lazure, P., Dumas, F., 2008. An external-internal mode coupling for a 3d hydrodynamical model for applications at regional scale (MARS). Adv. Water Resources 31, 233–250.

Leibovich, S., 1980. On wave-current interaction theory of Langmuir circulations. J. Fluid Mech. 99, 715–724.

Lentz, S. J., Howd, M. F. P., Fredericks, J., Hathaway, K., 2008. Observations and a model of undertow over the inner continental shelf. J. Phys. Oceanogr. 38, 2341–2357.
URL http://ams.allenpress.com/archive/1520-0485/38/11/pdf/i1520-0485-38-11-2587.pdf

Longuet-Higgins, M. S., 1953. Mass transport under water waves. Phil. Trans. Roy. Soc. London A 245, 535–581.

Longuet-Higgins, M. S., 1967. On the wave-induced difference in mean sea level between the two sides of a submerged breakwater. J. Mar. Res. 25, 148–153.

Longuet-Higgins, M. S., 2005. On wave set-up in shoaling water with a rough sea bed. J. Fluid Mech. 527, 217–234, an audio recording of a conference by Longuet-Higgins on this topic is available at http://av.fields.utoronto.ca:8080/ramgen/03-04/waterwaves/longuet-higgins.rm.
URL http://av.fields.utoronto.ca:8080/ramgen/03-04/waterwaves/longuet-higgins.rm

Longuet-Higgins, M. S., Stewart, R. W., 1964. Radiation stress in water waves, a physical discussion with applications. Deep Sea Research 11, 529–563.

Lubin, P., Vincent, S., Abadie, S., Caltagirone, J.-P., 2006. Three-dimensional large eddy simulation of air entrainment under plunging breaking waves. Coastal Eng. 53, 631–655.

Magne, R., Belibassakis, K., Herbers, T. H. C., Ardhuin, F., O'Reilly, W. C., Rey, V., 2007. Evolution of surface gravity waves over a submarine canyon. J. Geophys. Res. 112, C01002.

Marin, F., 2004. Eddy viscosity and Eulerian drift over rippled beds in waves. Coastal Eng. 50, 139–159.

Marsaleix, P., Auclair, F., Floor, J. W., Hermann, M. J., Estournel, C., Pairaud, I., Ulses, C., 2008. Energy conservation issues in sigma-coordinate free-surface ocean models. Ocean Modelling 20, 61–89.

McIntyre, M. E., 1981. On the 'wave momentum' myth. J. Fluid Mech. 106, 331–347.

McWilliams, J. C., Restrepo, J. M., Lane, E. M., 2004. An asymptotic theory for the interaction of waves and currents in coastal waters. J. Fluid Mech. 511, 135–178.

Mellor, G., 2002. Oscillatory bottom boundary layers. J. Phys. Oceanogr. 32, 3075–3088.

Mellor, G., 2003. The three-dimensional current and surface wave equations. J. Phys. Oceanogr. 33, 1978–1989, corrigendum, vol. 35, p. 2304, 2005, see also Ardhuin et al., vol. 38, 2008.

Mellor, G. L., 2008. The depth-dependent current and wave interaction equations: A revision. J. Phys. Oceanogr. 38, 2587–2596.
URL http://ams.allenpress.com/archive/1520-0485/38/11/pdf/i1520-0485-38-11-2587.pdf

Newberger, P. A., Allen, J. S., 2007a. Forcing a three-dimensional, hydrostatic, primitive-equation model for application in the surf zone: 2. application to DUCK94. J. Geophys. Res. 112, C08019.

Newberger, P. A., Allen, J. S., 2007b. Forcing a three-dimensional, hydrostatic primitive-equation model for application in the surf zone, part 1: Formulation. J. Geophys. Res. 112, C08018.

Péchon, P., Teisson, C., 1994. Numerical modelling of the three-dimensional wave-driven currents in the surf zone. In: Proceedings of the 24th international conference on coastal engineering, Kobe, Japan. ASCE, New York, pp. 2503–2512.

Phillips, O. M., 1977. The dynamics of the upper ocean. Cambridge University Press, London, 336 p.

Rascle, N., 2007. Impact of waves on the ocean circulation (impact des vagues sur la circulation océanique). Ph.D. thesis, Université de Bretagne Occidentale, available at http://tel.archives-ouvertes.fr/tel-00182250/.
URL http://tel.archives-ouvertes.fr/tel-00182250/

Rascle, N., Ardhuin, F., 2009. Drift and mixing under the ocean surface revisited. stratified conditions and model-data comparisons. J. Geophys. Res. 114, C02016, doi:10.1029/2007JC004466.

Rascle, N., Ardhuin, F., Queffeulou, P., Croizé-Fillon, D., 2008. A global wave parameter database for geophysical applications. part 1: wave-current-turbulence interaction parameters for the open ocean based on traditional parameterizations. Ocean Modelling 25, 154–171, doi:10.1016/j.ocemod.2008.07.006.
URL `http://hal.archives-ouvertes.fr/hal-00201380/`

Rascle, N., Ardhuin, F., Terray, E. A., 2006. Drift and mixing under the ocean surface. a coherent one-dimensional description with application to unstratified conditions. J. Geophys. Res. 111, C03016, doi:10.1029/2005JC003004.

Reniers, A. J. H. M., Roelvink, J. A., Thornton, E. B., 2004. Morphodynamic modeling of an embayed beach under wave group forcing. J. Geophys. Res. 109, C01030, doi:10.1029/2002JC001586.

Rivero, F. J., Arcilla, A. S., 1995. On the vertical distribution of $\langle\widetilde{u}\widetilde{w}\rangle$. Coastal Eng. 25, 135–152.

Shchepetkin, A. F., McWilliams, J. C., 2003. A method for computing horizontal pressure-gradient force in an oceanic model with nonaligned vertical coordinate. J. Geophys. Res. 108 (C3), 3090, doi:10.1029/2001JC001047.

Shchepetkin, A. F., McWilliams, J. C., 2004. The regional oceanic modeling system: A split-explicit, free-surface, topography-following-coordinate ocean model. Ocean Modelling 9 (C3), 347–404, doi:10.1029/2001JC001047.

Smith, J. A., 2006. Wave-current interactions in finite-depth. J. Phys. Oceanogr. 36, 1403–1419.

Svendsen, I. A., Putrevu, U., 1994. Nearshore mixing and dispersion. Proc. Roy. Soc. Lond. A 445, 561–576.

Thornton, E. B., Guza, R. T., 1983. Transformation of wave height distribution. J. Geophys. Res. 88 (C10), 5,925–5,938.

Tolman, H. L., 2008. A mosaic approach to wind wave modeling. Ocean Modelling 25, 35–47.

Tolman, H. L., 2009. User manual and system documentation of WAVEWATCH-III^{TM} version 3.14. Tech. Rep. 276, NOAA/NWS/NCEP/MMAB.

Uchiyama, Y., McWilliams, J. C., Restrepo, J. M., 2009. Wave-current interaction in nearshore shear instability analyzed with a vortex force formalism. J. Geophys. Res. 114, C06 021.

Uchiyama, Y., McWilliams, J. C., Shchepetkin, A. F., 2010. Wavecurrent interaction in an oceanic circulation model with a vortex-force formalism: Application to the surf zone. Ocean Modelling 34, 16–35.

Walstra, D. J. R., Roelvink, J., Groeneweg, J., 2000. Calculation of wave-driven currents in a 3D mean flow model. In: Proceedings of the 27th international conference on coastal engineering, Sydney. Vol. 2. ASCE, pp. 1050–1063.

Weber, J. E., Melsom, A., 1993. Transient ocean currents induced by wind and growing waves. J. Phys. Oceanogr. 23, 193–206.

Xia, H., Xia, Z., Zhu, L., 2004. Vertical variation in radiation stress and wave-induced current. Coastal Eng. 51, 309–321.